THE ASTROPHYSICAL JOURNAL, 382:382–395, 1991 December 1

INFRARED IMAGES, VIRGO SPIRALS, AND THE TULLY-FISHER LAW

R. F. PELETIER AND S. P. WILLNER
Harvard-Smithsonian Center for Astrophysics, 60 Garden Street, Cambridge, MA 02138
Received 1990 December 10; accepted 1991 June 4

ABSTRACT

For a complete (but magnitude-limited) sample of Virgo Cluster spiral galaxies, we present 1.65 μm photometry derived from images. Both galaxy inclinations and H-magnitudes are derived from the new data. The new photometry agrees with previous measurements. The infrared inclinations from the present data are usable for galaxies having inclinations greater than 45°, but deeper images would be needed for galaxies more face-on than this. The inclinations are the major observational uncertainty in the Tully-Fisher relation, but the relation in Virgo must have an intrinsic dispersion amounting to ∼0.4 mag. Sample selection is critical for determination of the intrinsic dispersion.

Subject headings: galaxies: clustering — galaxies: distances — infrared: sources — photometry

1. INTRODUCTION

Galaxy distances determined by means other than redshift are important for a number of reasons. Irregularities in the Hubble flow trace irregularities in the mass distribution and may reveal mass anomalies that do not appear in the distribution of luminous matter (e.g., Aaronson et al. 1982a; Lynden-Bell et al. 1988). Cosmological models themselves can be tested by the predicted velocity correlation tensor (Groth, Juszkiewicz, & Ostriker 1989) or the "cosmic Mach number" (Ostriker & Suto 1990), but comparison with observation requires that galaxy distances be known. Finally, the galaxy distances form part of the basis of the distance scale itself, and improved distance measurements may lead to a better value for the Hubble parameter.

One of the most useful ways to measure spiral galaxy distances involves comparison of the photometric brightness with the rotation velocity width (Tully & Fisher 1977). The latter is essentially a measure of the galaxy mass, so if the mass-to-light ratio is uniform, the intrinsic brightness ought to be determinable for any disk galaxy. The galaxy brightness is typically measured either in blue light (Tully & Fisher 1977; Bottinelli et al. 1983; Richter & Huchtmeier 1984; Bottinelli et al. 1987; Richter, Tammann, & Huchtmeier 1987; Pierce & Tully 1988, hereinafter PT; Kraan-Korteweg, Cameron, & Tammann 1988, hereinafter KCT; Sandage 1988; Fouqué et al. 1990) or at 1.65 μm in the infrared (Aaronson, Huchra, & Mould 1979, hereinafter AHM; Aaronson, Mould, & Huchra 1980, hereinafter AMH; Mould, Aaronson, & Huchra 1980; Aaronson et al. 1982b; Aaronson et al. 1986; PT; Bottinelli, Gouguenheim, & Teerikorpi 1988b), though other wavelengths of visible light have recently become popular (e.g., Bothun & Mould 1987, hereinafter BM; PT). Infrared measurements have the advantages that interstellar extinction, both in our galaxy and internal to the distant galaxy, is negligible (Aaronson & Mould 1986) and that recently formed stars, which may constitute a minor fraction of the mass but a large fraction of the blue light, will have little effect (AHM). Extinction can be especially large in edge-on galaxies, but these are just the ones most useful for measuring distances because the inclination corrections to the rotation velocities are small. These advantages may be partially offset by the steeper slope of the infrared relation, but in a direct comparison the scatter in the Tully-Fisher relation was smaller in the infrared than in the blue (PT), though Bottinelli et al. (1988b) and Sandage (1988) suggest that the scatter at the two wavelengths is not very different.

To date, galaxy infrared photometry has been performed with single detectors. Photometry using infrared arrays has several potential advantages, similar to those discussed by BM and PT for CCD observations. Arrays make it much easier to achieve the large angular fields of view required. Infrared images also provide an independent measure of the galaxy inclination angle, critical for determining the intrinsic velocity width, and one that is less subject to errors caused by dust extinction. Finally, the size of the galaxy can be determined directly from the infrared images and need not be extrapolated from images in visible light.

This paper reports an initial attempt to apply infrared array photometry to galaxies in the Virgo Cluster. The galaxies are all presumed to be at the same distance (to within an rms modulus of 0.14 mag—PT), so we have a test of whether array observations can improve distance measurements. This paper is primarily concerned with testing the methods and determining the scatter in the relation, so some of the analysis differs from other papers (e.g., Fouqué et al. 1990) which are primarily concerned with obtaining the best possible distance estimate.

2. SAMPLE SELECTION

Sample selection is critical to any test of the Tully-Fisher relation.[1] For present purposes, the sample of galaxies studied must satisfy two criteria. First, all must be at effectively the

[1] Whether sample selection is critical to the *use* of the Tully-Fisher relation to determine distances is, surprisingly, a matter of controversy. The danger is that magnitude-limited samples preferentially contain intrinsically bright galaxies, inducing a bias similar to Malmquist bias (Teerikorpi 1984, 1987). KCT showed that some earlier samples unaccountably lacked galaxies fainter than the mean Tully-Fisher relation but brighter than the supposed magnitude cutoff. Bottinelli et al. (1988a) argued in some detail that cluster incompleteness bias affects many previous results, but Tully (1988a) countered that the apparent bias problem is due to a local velocity anomaly. Schechter (1980), Teerikorpi (1984), and Tully (1988a) have shown that using magnitudes rather than velocity widths as the independent variable yields unbiased distance estimates provided the samples are unbiased in velocity width. Whether real samples satisfy this criterion is not clear (Bottinelli et al. 1986; Fouqué et al. 1990). Kraan-Korteweg, Cameron, & Tammann (1986) found evidence that existing samples were biased against galaxies with large velocity width, while other samples have been explicitly selected on the basis of line width (e.g., Bothun et al. 1985). Fouqué et al. (1990) found that either choice of independent variable gives the same distance if the sample is sufficiently complete and discussed in detail the biases that result if it is not. This paper is concerned with the scatter about the mean Tully-Fisher relation rather than the correct slope and intercept, so for our purposes the question of bias in the distances is not important.

same distance, so any dispersion can be attributed to the measurements and/or intrinsic dispersion in galaxy properties and not to different distances. Secondly, the sample must be unbiased in the sense that galaxies should not be excluded from the sample except by criteria applicable to galaxies of unknown distance. These requirements are to some extent incompatible, since the first requires that we exclude galaxies known to be in the foreground or background. Nevertheless, a sample of galaxies in the Virgo cluster can provide a worthwhile test.

In defining a sample of Virgo cluster spirals, we have started with the magnitude-limited sample studied in CO by Kenney & Young (1988). This consists of galaxies within the rectangle defined by $4° \leq \delta \leq 20\overset{\circ}{.}5$, $12^h \leq \alpha \leq 13^h$, classified Sa–Sd by Binggeli, Sandage, & Tammann (1985) or Sandage & Tammann (1981), and with magnitude $B_T^0 \leq 12.0$. Our sample is thus limited to galaxies brighter than the cluster mean $B_T^0 = 12.8$ (Fouqué et al. 1990) and would be subject to considerable population incompleteness bias if used to determine a distance by regression on velocity width (Teerikorpi 1987). Also, the use of blue magnitudes rather than infrared magnitudes to select the sample produces some bias against galaxies with significant internal extinction or high metallicity. Nevertheless, this sample should be adequate for testing measurement methods and for limiting the residual scatter.

The structure of the Virgo Cluster is complex and controversial. De Vaucouleurs & de Vaucouleurs (1973) distinguished not only between the main Virgo Cluster (Virgo I) and the Virgo II Cloud to the south, but also between the S, S′, and E clouds within Virgo I. Binggeli, Tammann, & Sandage (1987) lumped the S and E clouds into "Cluster A" and defined a "Cluster B" that seems to be the same as the S′ cloud. De Vaucouleurs & Corwin (1986) considered the S′ cloud to be behind the S cloud (0.37 mag greater distance modulus) and the X cloud, that is, galaxies south of $\delta = 5°$, not to be a physical grouping but to be on average at about the same distance as the S′ cloud. Fouqué et al. (1990) concurred in placing the S′ cloud behind the S cloud. Binggeli et al. (1987) agreed that there is evidence for Cluster B being behind A but pointed out that M 49 (≡NGC 4472), the central galaxy of B, must then be overluminous compared to M 87 (≡NGC 4486), even though the latter has characteristics of a luminous first-ranked cluster galaxy. Tonry, Ajhar, & Luppino (1990) placed M 49 about 0.2 mag beyond the Virgo Cluster mean distance, implicitly accepting the overluminosity that results. In contrast, Tully & Shaya (1984) found two out of three X cloud galaxies and two out of four S′ cloud galaxies to be nearer than the mean Virgo distance. There is also a more distant "M cloud" in the western part of the cluster within 6° of M 87 (Ftaclas, Fanelli, & Struble 1984), but most galaxies in this cloud are too faint to appear in our sample.

For this paper, we have not excluded any galaxies by reason of cloud membership. Table 1 gives our final list of sample galaxies, which consist of 23 S cloud galaxies, four galaxies in

TABLE 1

VIRGO SPIRAL GALAXIES IN S, S′, X SAMPLE

NGC (1)	Cloud (2)	v_{hel} (3)	d_{M87} (4)	Type (5)	B_T^0 (6)	I_{HI} (7)	ΔV_{20} (8)	ΔV_{50} (9)
4178	S	370	4.77	8	11.35	56.2	289	248
4192	S	472	4.94	2	10.31	81.3	465	456
4216	S	138	3.82	3	10.29	30.9	544	514
4254	S	2409	3.62	5	10.13	77.6	270	226
4298	S	1146	3.22	5	11.75	17.0	273	232
4302	S	1149	3.17	5	11.86	25.1	383	360
4303	X	1565	8.24	4	9.95	89.1	178	156
4312	S	130	3.77	2	11.97	1.8	227	208
4321	S	1580	3.96	4	9.89	49.0	272	251
4380	S	966	2.75	3	11.98	2.6	278	278
4388	S	2500	1.29	3	11.20	6.3	385	365
4394	S	917	5.96	3	11.47	6.5	176	162
4402	S	236	1.38	3	12.01	6.8	292	252
4419	S	−273	2.82	1	11.73	1.9	291	250
4450	S	1960	4.72	2	10.63	4.7	324	309
4501	S	2275	2.05	3	9.85	27.5	538	505
4527	X	1735	9.78	4	10.92	85.1	390	360
4532	S′	2010	5.99	10	11.69	43.7	230	158
4535	S′	1962	5.14	5	10.22	85.1	289	267
4536	X	1805	10.26	4	10.52	70.8	345	328
4548	S	490	2.39	3	10.72	10.5	264	235
4571	S	340	2.38	7	11.63	12.6	180	156
4579	S	1520	1.82	3	10.31	9.3	366	361
4639	S	980	3.14	4	11.88	14.5	313	280
4647	S	1415	3.28	5	11.82	7.1	240	197
4651	S	800	5.14	5	10.99	56.2	389	361
4654	S	1038	3.36	6	10.82	49.0	299	282
4689	S	1620	4.46	4	11.34	7.4	206	184
4698	S′	1010	5.89	2	11.15	28.2	435	416
4713	S′	650	8.54	7	11.83	51.3	196	165
4808	X	770	10.23	6	11.93	69.2	267	259

KEY TO COLUMNS.—(2) cluster membership status (see text); (3) heliocentric velocity, usually determined from H I measurements (Huchtmeier & Richter 1989); (4) distance from M 87 in degrees; (5) galaxy morphological type (de Vaucouleurs & Pence 1979); (6) total blue magnitude corrected for inclination and extinction (RC2); (7) integrated H I flux in Jy km s^{-1} (Huchtmeier & Richter 1989); (8) and (9) H I velocity widths at 20% and 50% of peak intensity (Huchtmeier & Richter 1989).

the S′ cloud, and four galaxies in the X cloud. All but six of the galaxies are within 6° of M 87, which has been considered a prime criterion for membership (Tully & Shaya 1984).[2] Fouqué et al. (1990) have used similar membership criteria and include in their sample all the galaxies in ours except NGC 4713, which is farther than 6° from the cluster center, and the four X cloud members. They include many fainter galaxies down to the limit for spirals in the cluster of $B_T^c \approx 16.5$. Ftaclas et al. (1984) list one galaxy in our sample, NGC 4254, as an M cloud member, but de Vaucouleurs (1982) considers this galaxy to be a valid S cloud member. De Vaucouleurs (1982) also lumps NGC 4535 and 4698 into the S cloud, though de Vaucouleurs & Corwin (1986) put them in S′. Of the galaxies we consider to be in the S cloud, de Vaucouleurs (1982) or de Vaucouleurs & Corwin (1986) specifically list all but NGC 4312, 4402, and 4419 as S cloud members. These three are low-velocity galaxies close to the cluster center, and we take them to be members.

In addition to position and brightness criteria, we have also excluded four galaxies classified S0 or S0/a by de Vaucouleurs & Pence (1979),[3] the interacting pair NGC 4567/4568, whose velocity widths may be disturbed by the interaction, and NGC 4438 for the same reason. NGC 4569 was excluded because it is either in the foreground (Tully & Shaya 1984) or has an anomalously small H I rotation width (Stauffer, Kenney, & Young 1986). The galaxies NGC 4235 and 4378 were excluded because they have been claimed to be in the background (Kenney & Young 1988), and we did not observe them. However, NGC 4532, which we did observe, was retained in spite of the same claim having made (de Vaucouleurs & Corwin 1986). Finally, the H I profiles of all galaxies were inspected to find out whether enough H I was detected to get a good estimate of velocity width. We have excluded three additional galaxies that were very faint in H I or had asymmetric velocity-position diagrams, usually disturbed by galactic H I: NGC 4064, 4212, and 4424. Table 2 lists all galaxies excluded from the sample and the reason.

All of our exclusions agree with those of Fouqué et al. (1990) except for NGC 4438 and 4569. (Some of our excluded galaxies are tabulated by Fouqué et al. but lack or have low quality—"d"—H I data.) For NGC 4438, Fouqué et al. apparently do not consider the evidence of interaction strong enough, though they do note that the H I data are of low ("c") quality. For NGC 4569, they derive a distance modulus 0.7 mag less than for the cluster mean, consistent with either a foreground location or anomalous velocity width. PT also excluded this galaxy from their sample. Including this galaxy in our sample would increase the derived scatter.

3. OBSERVATIONS

All of the observations were made with the Smithsonian Observatory Near Infrared Camera (SONIC) at the Mount Hopkins 24 inch (61 cm) telescope. The camera uses a 62 × 58 pixel indium antimonide detector manufactured by Santa Barbara Research Center. The image scale at the detector was 3″.55 pixel^{-1}, determined by measuring the positions of stars in the open cluster M 67 (Fagerholm 1906).

The observing procedure was to obtain an alternating series of images on the galaxy and at an adjacent sky position. At each position, the on-chip integration time was 30 s, and two successive on-chip integrations were added together. The "object" images were guided, and positional constancy was maintained to a fraction of a pixel. The "sky" positions were chosen to be $\gtrsim 5'$ away from the object position and to avoid bright stars. Larger offsets were used when galaxy size required. Successive settings on the sky were deliberately made at positions differing by several pixels, and the exposures were unguided, leading to drifts as large as a pixel. The individual pairs of object and sky exposures were recorded for later reduction.

For the larger galaxies, object exposures were made at more than a single position. Accurate offsetting was not possible at the telescope, so offsets were determined later from the position of the galaxy nucleus or field stars on the off-center frames.

In addition to data frames, the current was measured by inserting a cold blocker in the camera and measuring the signal in a series of 30 s integration times. Electronic offsets were measured by 0.2 or 0.27 s integrations with the blocker in

[2] The position of M 87 is 12^h28^m, $+12°.7$. Alternate cluster centers at 12^h27^m, $+13°.5$ (de Vaucouleurs & de Vaucouleurs 1973) or 12^h25^m, $+13°.1$ (Binggeli et al. 1987) have been preferred by other investigators.

[3] There is no ambiguity about omitting any of the four galaxies, which are NGC 4293, 4526, 4710, and 4866. The first three must be omitted for lack of H I. Bingelli et al. (1985) classify NGC 4293 as Sa pec, agree that NGC 4526 is S0, and do not include NGC 4710 and 4866 in their sample.

TABLE 2

Galaxies Omitted from Virgo Spiral Sample

NGC (1)	v_{hel} (2)	Type (3)	I_{HI} (4)	ΔV_{20} (5)	Reason omitted (6)
4064	927	1	1.0	...	Weak H I
4212	2076	4	>7.0	282	Galactic H I interference (Helou et al. 1984)
4235	2410	1	4.4	344	Weak H I; may be background (Kenney & Young 1988)
4293	891	0	<1.0	382	Type S0; no H I
4378	2555	1	10.4	367	May be background (Kenney & Young 1988)
4424	440	1	2.9	105	Faint, narrow H I
4438	70	0	8.2	360	Interacting; type S0
4526	450	−2	<2.8	347	Type S0; no H I
4567	2270	4	17.1	315	Interacting with NGC 4568
4568	2255	4	19.1	350	Interacting with NGC 4567
4569	−220	2	8.8	381	Foreground (Tully & Shaya 1984) or stripped H I (Stauffer et al. 1986)
4710	1125	−1	<0.6	...	Type S0; no H I
4866	1988	−1	18.2	557	Type S0

Key to columns.—(2) heliocentric velocity; (3) morphological type; (4) H I flux in Jy km s^{-1}; (5) velocity width at 20% of peak. References are the same as for Table 1.

place. Flat fields were measured by pointing the telescope at the dome illuminated by incandescent light bulbs. Standard stars (Elias et al. 1982) were also observed for photometric calibration. For these observations, the detector temperature was 30 K and the bias was 200 mV. A nonlinearity correction was measured by observing signal as a function of integration time for constant detector illumination; in practice, the measured correction was less than 2% and was not applied.

Images were calibrated with the aid of the IRAF package from NOAO. Dark current was subtracted from all images. An average sky image was formed for each object by normalizing and median filtering all sky images associated with that object. We found experimentally that the sky variation time scales were so short that an adjacent sky frame gave better sky subtraction than the average sky. Accordingly, the average sky was used to clean field stars from individual sky frames, and an adjacent cleaned sky frame was then subtracted from each object frame. The result was divided by a normalized flat field, and bad pixels were masked. A deficiency in SONIC was that the detector temperature was insufficiently regulated, and the typical variations of 0.05 K led to dark current variations of 200 e^{-} s^{-1} $pixel^{-1}$. Fortunately, the dark current has a known pattern and displays a systematic difference between odd and even columns. We corrected for the odd-even effect by subtracting an average row from the data after filtering out the objects. The residual pattern was removed by subtracting every linear combination of sky frames from the data and choosing the output frame that least resembled the residual dark. This procedure worked well most of the time, although a few object frames could not be adequately corrected and had to be thrown away. The final step was to mosaic any frames taken at multiple positions in the same galaxy.

All data reported here were taken on photometric nights, as evidenced by the agreement of standards throughout the night and the lack of visible clouds. Variance among standards was 0.02 mag (after extinction correction of ≈ 0.1 mag per air mass), some of which may be due to inaccuracy in the standard star system. We have insufficient data to determine a correction from the natural photometric system to the CIT system (Elias et al. 1982), but because of the sharpness of the atmospheric and filter cutoffs, the correction is probably negligible. (The bandpass filter was part of the batch purchased from Barr Associates in 1987 by NOAO and many other astronomical institutions.)

Even though we imaged areas out to $\sim 0.5 D_0$ in most galaxies, the coverage was usually smaller than the $\sim 2 D_0$ that would be needed to determine total magnitudes.[4] Instead, we determined the flux inside both circular and elliptical apertures with diameters going up to $0.5 D_0$. Bright stars were seldom a problem but when necessary were eliminated by interpolating over the contaminated pixels.

Ellipticities and position angles of galaxies were determined on the frames by using a two-dimensional ellipse fitting package, GALPHOT, written by M. Franx at the CfA. The package gives radial profiles of ellipticity and major axis position angle. We averaged these parameters radially in the outer regions of each galaxy to obtain an average ellipticity and position angle. To measure the light in each aperture, the galaxy center was found with a central moment method interpolating over fractions of pixels. The uncertainty in an aperture magnitude consists of sky background errors and random pixel variations, mainly caused by dark current residuals. In most cases the sky could be determined accurately on our frames, so that sky background errors usually did not exceed 0.03 mag. The random pixel fluctuations were negligible except for some small apertures. Table 3 lists the H-magnitudes in circular beams of diameter $\log(A/D_0) = -0.5$ ($\Rightarrow A/D_0 = 0.316$). The uncertainties are taken to be at least 0.05 mag in order to allow for calibration errors. The rms uncertainty for the entire sample is shown in the last row of Table 3.

Magnitudes in elliptical rather than circular beams might be expected to produce a Tully-Fisher relation with lower scatter. Elliptical magnitudes more closely resemble isophotal magnitudes, and sky errors affect them less. Table 3 lists derived ellipticities, position angles, and magnitudes measured in elliptical beams. The major axes of the ellipses were taken as log $(A/D_0) = -0.5$, the same size as the circular beam, and also as $A/D_0 = 0.5$, that is, a factor of 1.6 larger.

A third set of magnitudes was determined entirely from the infrared data. These are isophotal magnitudes H_μ, defined as the total light inside an isophote $H = \mu$ mag arcsec^{-2}. Table 3 tabulates H_{19}, which is a compromise between including most of the galaxy but minimizing sky background errors. Section 5.1 compares the Tully-Fisher relations derived from the various kinds of magnitudes.

4. COMPARISON WITH PREVIOUS RESULTS

4.1. *Photometry*

Most of the infrared photometry used for Tully-Fisher purposes has come from Aaronson et al. (1982b) and references therein. The data consist of aperture photometry, with measurements in a few apertures per galaxy, for more than 300 galaxies. The measurements were interpolated to derive magnitudes within a circular area of diameter A such that $\log(A/D_1) = -0.5$.[5] In order to establish the quality of our data, we determined array magnitudes in circular beams of this same size. Figure 1 demonstrates the good agreement between the array magnitudes and the single channel magnitudes. The mean difference of 0.006 mag and dispersion of 0.063 mag are within the rms uncertainty of our data, 0.066 mag. There is no noticeable dependence on galaxy magnitude. Aaronson et al. give an uncertainty in their individual aperture measurements of 0.03 mag, but interpolation (or extrapolation) to D_1 will introduce additional scatter, and our photometric system may differ slightly from theirs. The magnitude differences are thus, if anything, smaller than expected, and our magnitude uncertainties may be slightly exaggerated. In any case, photometric errors do not contribute significantly to the infrared Tully-Fisher scatter, as is the case at other wavelengths (BM).

KCT proposed a method of estimating H-magnitudes of galaxies from observed B-magnitudes and velocity widths. Our new data provide a test of this method. For 15 galaxies in their sample with previous *H-measurements*, our new measurements are 0.06 ± 0.09 brighter on average. (About half the systematic difference reflects our use of D_0 rather than D_1.) However, for nine galaxies with H-magnitudes *estimated* by KCT, our measurements are 0.58 mag brighter on average. The dispersion of

[4] Here D_0 is the isophotal diameter in the blue corrected for inclination of the galaxy and for extinction by dust. Values of D_0 were taken from the RC2 (de Vaucouleurs, de Vaucouleurs, & Corwin 1976).

[5] Here D_1 is the same as D_0 except that the corrections for inclination and for Galactic extinction differ slightly (AMH). The magnitudes in Table 3 are based on D_0, not D_1, and are 0.03 ± 0.02 mag brighter on average. Magnitudes in Fig. 1 are based on D_1.

TABLE 3

PHOTOMETRIC RESULTS

NGC (1)	D_0 (2)	$H_c^{-0.5}$ (3)	± (4)	$H_e^{-0.5}$ (5)	± (6)	$H_e^{+0.5}$ (7)	± (8)	H_{19} (9)	± (10)	ellipt. (11)	P.A. (12)
4178	250.2	10.07	0.05	10.91	0.05	10.35	0.05	10.67	0.06	0.82	34
4192	465.8	7.71	0.05	8.33	0.05	7.78	0.05	7.45	0.05	0.80	152
4216	378.6	7.28	0.05	7.54	0.05	7.23	0.05	7.01	0.05	0.72	20
4254	329.8	8.78	0.09	8.90	0.08	8.59	0.15	9.10	0.15	0.24	65
4298	173.0	9.12	0.05	9.87	0.05	9.31	0.05	9.12	0.05	0.39	135
4302	228.2	9.01	0.05	9.75	0.05	9.26	0.05	8.44	0.05	0.88	0
4303	370.0	7.73	0.05	7.91	0.05	7.57	0.06	7.63	0.07	0.30	0
4312	217.8	9.52	0.09	9.94	0.05	9.51	0.06	9.12	0.15	0.74	172
4321	424.8	7.80	0.13	7.98	0.11	7.51	0.19	7.54	0.33	0.29	115
4380	203.4	9.63	0.05	9.97	0.05	9.45	0.05	9.51	0.08	0.47	155
4388	238.8	8.77	0.05	9.04	0.05	8.67	0.05	8.65	0.05	0.63	90
4394	244.4	8.99	0.05	9.08	0.05	8.83	0.05	9.04	0.05	0.33	143
4402	194.2	9.49	0.05	10.19	0.05	9.52	0.05	9.00	0.08	0.80	90
4419	169.2	8.48	0.05	8.72	0.05	8.40	0.05	8.24	0.05	0.62	135
4450	280.6	8.05	0.05	8.25	0.05	7.92	0.05	7.92	0.05	0.45	0
4501	378.6	6.87	0.05	7.16	0.05	6.77	0.05	6.56	0.10	0.54	140
4527	314.8	7.73	0.05	8.05	0.05	7.71	0.05	7.48	0.05	0.71	70
4532	144.0	10.30	0.05	10.56	0.05	10.06	0.05	9.46	0.05	0.50	158
4535	396.4	8.39	0.13	8.68	0.05	8.03	0.05	8.29	0.31	0.30	35
4536	387.4	8.33	0.15	8.64	0.05	8.28	0.09	8.39	0.22	0.64	115
4548	322.2	7.91	0.05	8.44	0.10	8.20	0.22	8.42	0.06	0.25	95
4571	228.2	9.71	0.13	9.84	0.20	9.30	0.27	9.80	0.34	0.19	30
4579	322.2	7.59	0.05	7.68	0.05	7.43	0.06	7.49	0.10	0.30	73
4639	169.2	9.44	0.05	9.60	0.05	9.24	0.05	9.10	0.05	0.31	135
4647	181.2	9.52	0.05	9.65	0.05	9.15	0.05	9.18	0.11	0.21	125
4651	217.8	8.57	0.05	8.69	0.05	8.41	0.05	8.48	0.05	0.31	79
4654	262.0	8.89	0.05	9.18	0.05	8.72	0.05	8.70	0.09	0.48	123
4689	244.4	9.67	0.06	9.82	0.06	9.25	0.08	8.96	0.12	0.22	170
4698	233.4	8.40	0.05	8.54	0.05	8.21	0.05	8.23	0.05	0.39	160
4713	157.8	10.50	0.07	10.68	0.06	10.16	0.10	10.63	0.15	0.27	92
4808	140.6	9.94	0.05	10.37	0.05	9.85	0.05	9.33	0.14	0.62	130
Photometry of additional galaxies not included in sample:											
4064	233.4	9.29	0.05	9.56	0.05	9.25	0.05	9.39	0.07	0.64	155
4212	173.0	9.26	0.05	9.51	0.05	8.94	0.05	8.68	0.08	0.37	72
4293	322.2	8.08	0.05	8.44	0.05	7.96	0.05	7.51	0.06	0.56	79
4424	203.4	9.81	0.09	10.07	0.06	9.68	0.10	9.70	0.20	0.51	101
4438	476.6	7.76	0.05	7.79	0.05	7.74	0.05	7.88	0.05	0.45	23
4526	353.4	7.16	0.05	7.42	0.05	7.14	0.05	7.01	0.05	0.67	115
4569	499.0	7.39	0.08	7.64	0.06	7.29	0.13	7.38	0.15	0.56	20
4710	233.4	8.40	0.05	8.94	0.05	8.41	0.05	7.84	0.08	0.80	29
4866	287.2	8.55	0.05	9.04	0.05	8.59	0.05	8.29	0.05	0.80	89
rms magnitude uncertainty			0.069		0.060		0.079		0.128		

KEY TO COLUMNS.—(2) isophotal diameter in arcsec (RC2); (3) H-magnitudes in a circular beam of diameter $0.316D_0$; (5) H-magnitudes in an elliptical beam with major axis diameter $0.316D_0$; (7) H-magnitudes in an elliptical beam with major axis diameter $0.5D_0$; (9) isophotal magnitudes within $H = 19$ mag arcsec^{-2}; (11) infrared ellipticity $(1 - r_{min}/r_{maj})$; (12) position angle of the major axis from N through E for the elliptical beams. Cols. (4), (6), (8), and (10) give the uncertainties of the magnitudes in the immediately preceding columns.

the estimated magnitudes around the systematic difference is 0.49 mag. Both the systematic difference and the dispersion are significantly larger than the 0.32 mag dispersion estimated by KCT.

4.2. *Velocity Widths*

The most convenient line for measuring galaxy rotation velocities is the 21 cm line of H I. (Optical emission lines—e.g., Rubin, Whitmore, & Ford 1988—or CO emission might also be used.) Ideally, complete synthesis images would be modeled to determine the rotation velocity (e.g., Guhathakurta et al. 1988), but more commonly the velocity width ΔV must be determined from the line width of the integrated spectrum of the galaxy.

Several prescriptions can be used for converting the observed spectrum to line width. The most common is to measure the velocity width at 20% of the peak intensity level, but some have used the 50% or even the 80% level (Lewis 1987). For this sample, we find that the choice makes little difference and have chosen the 20% level mainly for consistency with most other investigators and because more data are published in those terms. For each sample galaxy, all (except obviously discrepant) velocity widths from the catalog of Huchtmeier & Richter (1989) were averaged; the same was also done for the 50% widths to compare the results. The rms dispersion in the published 20% widths is 13.5 km s^{-1}. The adopted velocity widths are given in Table 1.[6]

[6] Some of the early single-dish spectra, especially those obtained with a small antenna, gave velocity widths discrepant from the mean by up to 40 km s^{-1}. These were omitted from the average when possible, but for some galaxies with few other measurements available, similar measurements were included. However, omitting these measurements did not change our results. The uncertainties of the more recent synthesis measurements are probably less than 13.5 km s^{-1}, but the value doesn't matter much because the overall uncertainty in most of the velocity widths is dominated by the uncertainty in the inclinations.

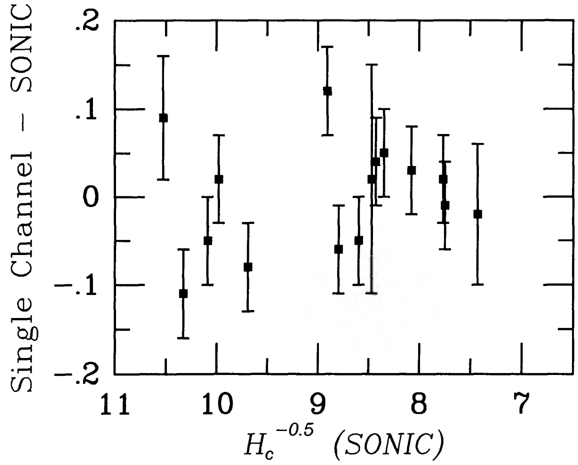

FIG. 1.—Comparison between SONIC magnitudes and magnitudes from single-detector aperture photometry (Aaronson et al. 1982b; Mould et al. 1980). For this figure only, SONIC magnitudes are measured in circular apertures of diameter A such that $\log (A/D_1) = -0.5$; D_1 values are from the references cited.

The H I line width found from integrated spectra includes a contribution from noncircular motions due to random motions of gas clouds (Lewis 1987) and possible large-scale irregularities in the H I distribution and velocity field. Noncircular motion might cause systematic errors or introduce nonlinearity into the Tully-Fisher relation. In our sample of bright galaxies the velocity widths are so large and their range so small that noncircular motions are unimportant. Bottinelli et al. (1988b) found the same for their galaxy sample even though it included fainter galaxies than ours. The effect of cluster environment on the velocity widths is also likely to be negligible (Guhathakurta et al. 1988).

4.3. *Inclinations*

To correct the velocity widths to their edge-on values, one needs to know the inclination of each galaxy. Four methods to determine the inclination can be found in the literature: (1) Rectification of images based on their photographic appearance (Danver 1942). (2) Conversion of axis ratios to inclinations, assuming an intrinsic galaxy thickness (Hubble 1926). The axis ratios may be measured photographically or on CCD images and may be measured at a particular isophote or over a range of isophotes. (3) A variation of the axis ratio method using a Fourier transform (Grosbøl 1985) to reduce sensitivity to nonbisymmetric irregularities. (4) Radio synthesis imaging of H I followed by fitting a kinematic model to the radial velocity pattern (Warner 1973; Guhathakurta et al. 1988; Warmels 1988). Method 2 is the most commonly used because the necessary data are most readily available, although the other methods may be preferable (AHM). However, none of the methods necessarily yields true inclinations. Method 1 suffers from asymmetries and axial ratio variations with radius; in methods 2 and 3, the assumption that the galaxy is intrinsically circular may be false, the observed axial ratios vary with radius, and the galaxy thickness is unknown; and in method 4, motions may be noncircular, and it is difficult to separate rotation velocities from warps and from the major axis position angle, especially if the synthesis data have insufficient spatial resolution. In using method 2, the intrinsic thickness is sometimes taken to be a function of galaxy type (Bottinelli et al. 1983; Fouqué et al. 1990) or is corrected (by 3°) for a suspected systematic error (AMH), but neither correction gives a significant change in sin (i) at inclinations $i > 45°$.

Since axis ratio variations are often caused by star-forming regions and dust lanes, features that are seen predominantly in visible light, the determination of inclinations might be improved by using the axis ratios in the H band. The observed axis ratios still vary with radius; Figure 2 shows some example profiles. For each galaxy in our sample, we have averaged the axis ratios from our images over the outer parts of the galaxies to determine a single ratio and transformed that ratio to inclination. The intrinsic disk thickness adopted was 0.15. The value of 0.2 used for visible images (e.g., AHM; Helou, Hoffman, & Salpeter 1984) is unacceptable because many galaxies have observed axis ratios greater than 0.8. The value for the disk thickness is not critical because it only matters for almost edge-on galaxies, but for these galaxies sin (i) is almost independent of i. The derived inclinations are given in Table 4, along with five other determinations of inclination angle.

Table 5 compares the scatter and systematic differences among five inclination determinations. All the methods based

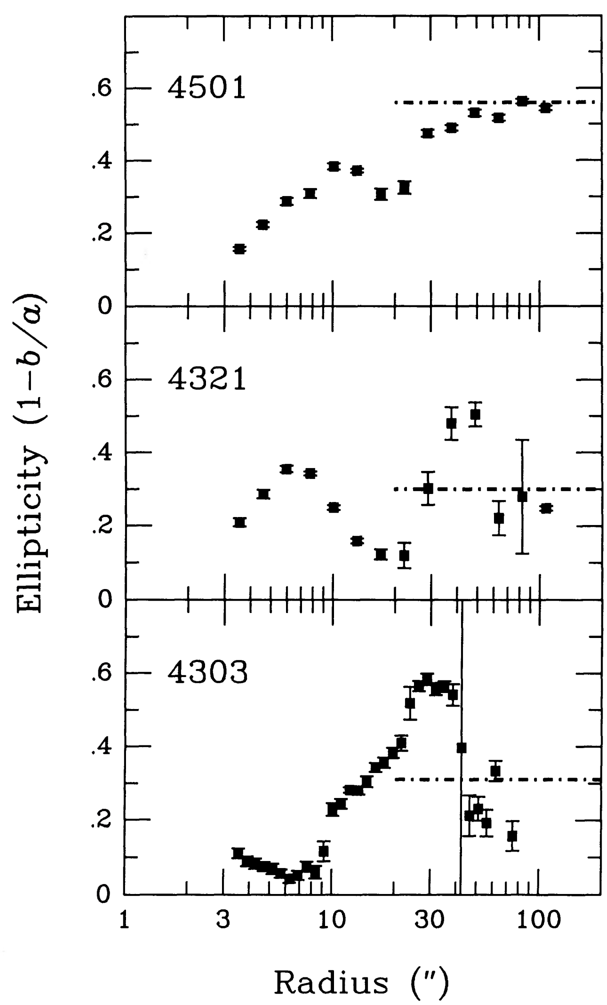

FIG. 2.—GALPHOT ellipticity profiles for three typical galaxies. The radius on the abscissa is $(r_{\rm maj} \times r_{\rm min})^{0.5}$, and ellipticity is $1 - r_{\rm min}/r_{\rm maj} \equiv 1 - b/a$. Horizontal dot-dash lines indicate the ellipticity adopted in determining the inclinations given in Table 4. NGC 4501 shows a smooth increase to a constant value at large radii. NGC 4321 and NGC 4303 show profiles that change a lot as a function of radius, even at the largest radii usable.

TABLE 4

GALAXY INCLINATION ANGLES

NGC (1)	Rectification (2)	Photographic (3)	CCD (4)	Fourier Transform Method (5)	Radio (6)	Infrared (7)
4178	...	72	78	...	62	84
4192	78	77	86	...	70	82
4216	81	83	90	...	63	76
4254	29	31	29	40	...	41
4298	...	58	...	55	...	53
4302	...	88	...	...	...	90
4303	5	28	...	35	...	46
4312	...	81	...	...	...	78
4321	31	31	25	25	30	45
4380	...	58	61	58	...	59
4388	81	82	83	...	...	70
4394	21	28	...	22	...	49
4402	82	78	...	...	...	82
4419	...	74	...	...	...	69
4450	53	48	48	50	37	58
4501	64	61	61	58	57	64
4527	70	75	...	...	...	75
4532	...	70	61	...	...	61
4535	42	46	45	48	40	46
4536	59	67	...	...	...	71
4548	...	39	35	42	38	42
4571	...	31	35	31	...	36
4579	...	39	42	39	36	46
4639	...	48	55	52	...	47
4647	...	39	40	40	36	38
4651	...	49	55	54	42	47
4654	...	55	58	56	49	60
4689	...	33	39	36	27	39
4698	...	60	62	46	...	53
4713	...	52	...	47	...	44
4808	...	67	...	...	...	69

KEY TO COLUMNS.—(2) Rectification based on photographic appearance (Danver 1942); (3) axis ratio from de Vaucouleurs & Pence (1979) converted to inclination via formula from Aaronson et al. (1980); (4) axis ratios as a function of radius from CCD data (PT); (5) Fourier transform method (Grosbøl 1985); (6) kinematic model fitted to radio synthesis maps (Guhathakurta et al. 1988; Warmels 1988); (7) axis ratios as a function of radius from the infrared data of this paper.

TABLE 5

INCLINATION DETERMINATIONS COMPARED TO PHOTOGRAPHIC INCLINATIONS

Method (1)	Number of Galaxies (2)	Systematic Difference (3)	RMS Spread (4)
All galaxies:			
Rectification	13	3.0	7.2
CCD	19	−1.8	4.6
Fourier Transform	19	0.0	5.3
Radio	10	6.8	5.1
Infrared	31	−2.3	7.8
Galaxies with $i_{pg} > 45°$:			
Rectification	9	0.8	4.4
CCD	12	−2.5	4.7
Fourier Transform	10	1.1	5.5
Radio	8	8.9	5.0
Infrared	22	0.5	6.1

KEY TO COLUMNS.—(1) Method being compared to i_{pg} (Table 4); (2) number of galaxies used in the comparison; (3) average difference in the sense $i_{pg} - i$; (4) rms scatter between these inclinations.

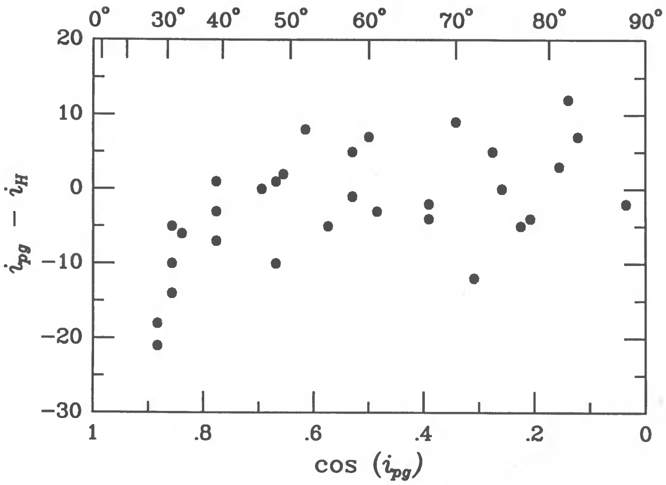

FIG. 3.—Inclinations determined from H-band axis ratios (i_H) compared with inclinations obtained from blue axis ratios (i_{pg}). The abscissa is the cosine of the inclination with the corresponding inclinations indicated at the top.

on axis ratios agree quite well overall, but the kinematic (H I) inclinations are systematically lower. Figure 3 compares the infrared and the photographic inclination angles, i_H and i_{pg}, in more detail. The agreement still looks good except at low inclinations, where three galaxies have i_H much higher than i_{pg}.[7] If our galaxy sample is complete and has no preferred orientation in space, the inclinations should be uniformly distributed in cos(i). Figure 4 shows that the infrared axis ratios give a deficiency of face-on galaxies, while photographic axis ratios give a similar, though smaller, deficiency.

The reason for the unduly high infrared inclinations can be seen in Figure 5, which compares the visible and infrared images of NGC 4303. This galaxy is nearly face-on, and its disk therefore has low surface brightness. The axis ratio measured in the infrared is that of a barlike feature and not of the disk at all. At present, images in visible light reach fainter surface brightness relative to galaxy disks and are able to detect even face-on disks. We expect that infrared images that reach equivalent surface brightness levels will give improved inclinations. Even the present values, however, are adequate for galaxies known a priori to have inclinations greater than 45°.

Intercomparison of different methods of measuring inclinations provides an estimate of the uncertainty in any one method. If the photographic, CCD, and infrared inclinations are assumed to have independent, normally distributed errors, the values of mutual rms scatter (Table 5, $i_{pg} > 45°$) imply *internal* uncertainties $\Delta i_{pg} = 1\overset{\circ}{.}2$, $\Delta i_{CCD} = 4\overset{\circ}{.}5$, and $\Delta i_H = 6\overset{\circ}{.}0$. If instead the three methods are assumed to have approximately equal scatter, as suggested by comparison with Fourier transform and radio inclinations and by the Tully-Fisher scatter derived below, $\Delta i = 4\overset{\circ}{.}4$. These estimates assume that systematic errors are negligible and thus give the *minimum* combined uncertainties.

Estimating the *external* uncertainties is more difficult, but the systematic discrepancy between all the axis ratio methods and the radio method (~9°) encourages us to be cautious. However, the radio method may suffer from systematic errors

[7] The three galaxies are NGC 4303, 4321, and 4394.

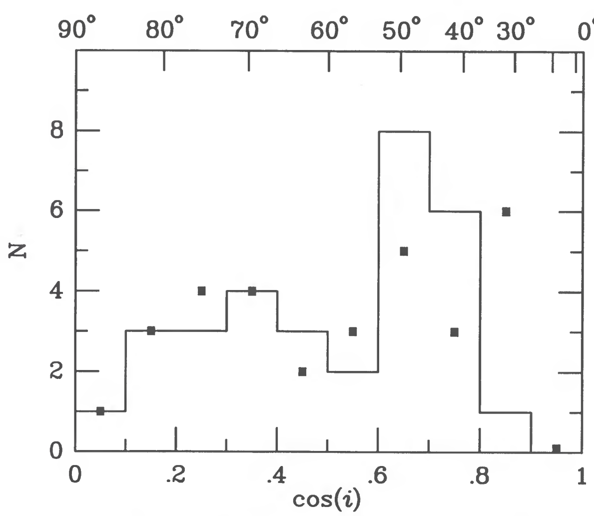

FIG. 4.—Histogram of the distribution of inclinations for the Virgo sample. Inclinations from photographic axis ratios are shown as squares, while infrared inclinations are shown as lines. If the galaxies are randomly oriented in space and there are no systematic errors in the inclinations, there should be equal numbers in each bin.

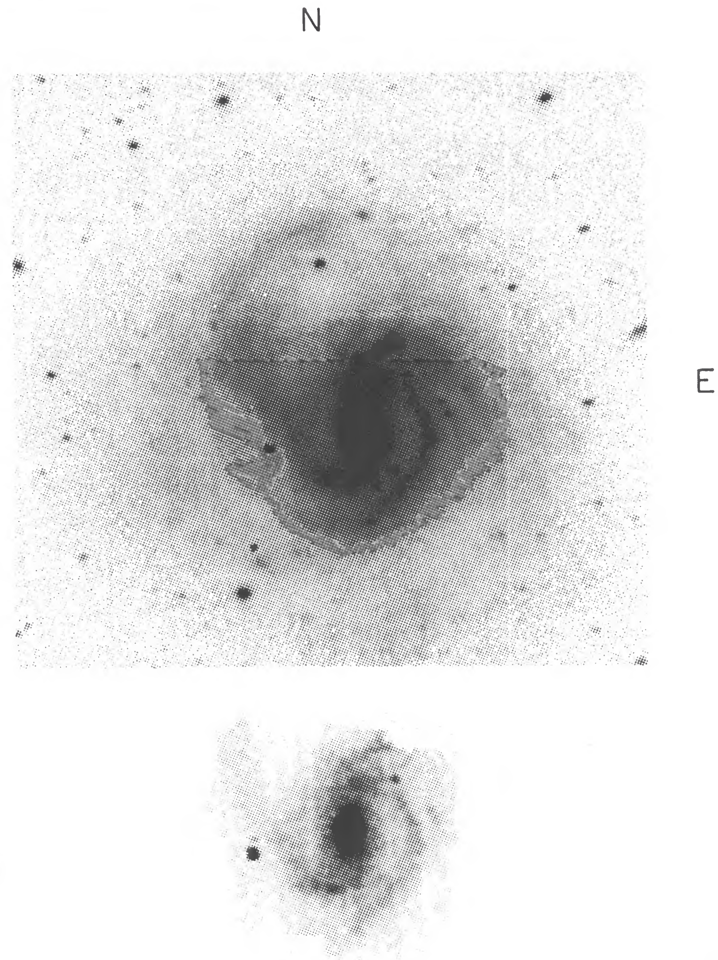

FIG. 5.—Gray-scale maps of NGC 4303 in H (*small image*) and V (*large image*). The angular scales are the same for both images, and celestial directions are indicated. The V-frame comes from a CCD image made available by R. Schild. The infrared image shows an elongated structure, while the deeper V-image shows in addition a more nearly circular disk of larger diameter.

of its own. When applied to eight galaxies of large angular size (Begeman 1987), the radio inclinations are on average 6° greater than inclinations determined from photographic axis ratios. This discrepancy is *opposite* the one found for Virgo Cluster galaxies. Ignoring the radio method, the systematic difference between photographic and rectification inclinations is 3°.0. We adopt an uncertainty of 5° for the galaxy inclinations, in agreement with the determinations of BM and Fouqué et al. (1990). Section 5.3 compares Tully-Fisher relations derived from different determinations of inclination and shows that this estimate is consistent with the observed scatter.

Why are the various inclinations so different? We think the answer is not the lack of data to measure them accurately, but the fact that the stars in a galaxy are not distributed regularly in a featureless disk. Bars, bulges, spiral arms, dust lanes, etc., all contribute to the intrinsic irregularities. Variation of axis ratio with radius is just one of the difficulties in determining inclinations, but Figure 2 illustrates the problem. One galaxy shown (NGC 4501) has a well-defined ellipticity in the outer parts, but the two others have axis ratios highly dependent on the radius range in which they are determined. Some samples of galaxies do show smaller dispersion in derived inclinations, for example, only 3°.1 for one sample of 16 well-studied galaxies (Bottinelli et al. 1983). This sample, however, was explicitly selected to have well-determined inclinations; indeed, one galaxy with a discrepancy of 19° was rejected from the sample for that reason alone.

4.4. *Tully-Fisher Relation*

The correct fitting method to derive distances from the Tully-Fisher relation is controversial (see note 1), but for determining the goodness of fit it is best to use a double regression technique (e.g., Cameron-Reed 1989) that explicitly takes into account uncertainties in both variables. Since the magnitude uncertainties are much smaller than the uncertainties in the velocity widths, a standard least-squares technique with the magnitude being the independent variable (as advocated by PT and Tully 1988a among others) would give essentially the same results. The uncertainties are most directly expressed as χ^2 per degree of freedom ("reduced χ^2" or $\chi^2_{\rm red}$), which gives a measure of the variance observed compared to the variance expected on the basis of known uncertainties in the variables. However, it is customary to express the scatter in the Tully-Fisher diagram as an uncertainty in magnitude, which translates directly into an uncertainty in galaxy distance. We have derived these uncertainties by adding (in an rms sense) to each galaxy measurement the amount of magnitude uncertainty needed to make the reduced χ^2 equal to unity. The result is a measure of the combined dispersions due to intrinsic differences among galaxies and to dispersion in galaxy distances.

A recent examination of the Virgo cluster was given by PT. Their sample has 20 galaxies in common with ours, although only 12 have previous infrared photometry. Table 6 compares their results with our new data for the same samples, both with and without the eight galaxies newly observed. Starting from the data they used (with infrared magnitudes from Aaronson et al. 1982b), the Tully-Fisher scatter successively decreases as we (1) remove corrections for nonrotational motion from the velocity widths, (2) replace the older H-magnitudes with our new ones, and (3) replace the older velocity widths ΔV_{20} with the newer, averaged data (Huchtmeier & Richter 1989). Thus our new H-magnitudes and the newer data on velocity widths are, if anything, superior to previous methods and do not increase the Tully-Fisher scatter. The inclinations are another matter. The CCD inclinations (PT) give significantly smaller scatter than the photographic inclinations, but even with the photographic inclinations, this sample shows intrinsic scatter $\lesssim 0.12$ mag. This amount of scatter is smaller than the expected depth of the Virgo cluster and is consistent with no intrinsic scatter at all in the Tully-Fisher relation itself, but the result applies only to the limited sample of 20 galaxies. Section 5.4 will show that the scatter is much larger when our complete sample is examined.

5. DISCUSSION

This section compares the Tully-Fisher relations derived from different kinds of data. We adopt an empirical attitude that whichever data give the least dispersion are "best." In

TABLE 6

TULLY-FISHER LAWS COMPARED WITH PT

Magnitudes (1)	Velocity Widths (2)	Inclinations (3)	$\chi^2_{\rm red}$ (4)	Magnitude Error (5)	Slope (6)	Intercept (7)
Sample with H-Magnitudes Given by PT (12 Galaxies):						
A82	W_R(PT)	PT	1.42	0.20	−0.106	2.522
A82	PT	PT	1.18	0.13	−0.096	2.571
Table 3	PT	PT	1.01	0.03	−0.097	2.569
Table 3	ΔV_{20}	PT	0.81	0.00	−0.098	2.568
Table 3	PT	pg	1.51	0.25	−0.099	2.572
Table 3	ΔV_{20}	pg	1.18	0.15	−0.100	2.571
Sample of All Galaxies in Common with PT (20 Galaxies):						
Table 3	W_R(PT)	PT	1.14	0.13	−0.107	2.524
Table 3	PT	PT	0.94	0.00	−0.097	2.573
Table 3	ΔV_{20}	PT	0.85	0.00	−0.095	2.575
Table 3	PT	pg	1.23	0.19	−0.096	2.578
Table 3	ΔV_{20}	pg	1.09	0.12	−0.095	2.580

KEY TO COLUMNS.—(1) Source of $H_c^{-0.5}$ magnitudes used; "A82" indicates magnitudes used by PT (Aaronson et al. 1982b); (2) source of velocity width: from Table 1 (ΔV_{20}) or from PT, uncorrected or corrected (W_R) for noncircular motions; (3) source of inclinations; (4) reduced χ^2 of fit; (5) additional uncertainty in the H-magnitudes necessary to bring $\chi^2_{\rm red}$ down to unity; (6) and (7) best-fit slope (a) and intercept (b) for $\log \Delta V = a(H - 9.0) + b$. The uncertainties in the slopes are very close to 0.009 for all fits, and the uncertainties in the intercepts are close to 0.011.

order to minimize the effects of inclination uncertainties, we consider only the 22 galaxies with photographic inclinations $i_{pg} \geq 45°$ except where otherwise stated.

5.1. *Circular, Elliptical, or Isophotal Magnitudes?*

The objective is to find the magnitude best correlated with the width of the rotation curve. The most common practice has been to measure within a circular diameter defined by a B-band isophote corrected for inclination effects. The correction arises because if an optically thin disk galaxy could be viewed from progressively more edge-on directions, a circular beam with a fixed metric diameter would contain a progressively larger fraction of the total light. Furthermore, the measured surface brightness would increase at all positions on the major axis and thus the derived isophotal diameter would increase. The former effect can be avoided by using elliptical beams, but the correction for the change in isophotal diameter (Heidmann, Heidmann, & de Vaucouleurs 1971) has to be applied for either elliptical or circular beams. There has been considerable discussion whether to apply this correction or not (related to optical thickness arguments; Tully 1972), but since galaxies in H are likely to be optically thin (Peletier & Willner 1991), we have applied a correction. In addition, a small correction has to be applied to correct the optically determined diameters for dust extinction in B. Diameters labeled D_0 in the RC2 have these corrections applied. Other authors (e.g., BM; PT) have discussed the best types of magnitudes to use in the *BVRI* bands and have reached varying conclusions. BM also pointed out that intrinsic differences in galaxy surface brightness profiles are a major source of scatter in Tully-Fisher distances when beam sizes less than D_0 are used.

We have analyzed the scatter in the Tully-Fisher relation for our sample using four different kinds of magnitudes: circular with diameter A chosen so that $\log(A/D_0) = -0.5$, elliptical with axis ratios determined from the infrared images and major axes A_{maj} such that $\log(A_{maj}/D_0) = -0.5$ and $A_{maj}/D_0 = 0.5$, and isophotal magnitudes H_{19}. Results are shown in Table 7. All fits imply that the scatter is larger than can be explained purely by the observational uncertainties, and an additional photometric uncertainty of $\gtrsim 0.45$ mag has to be added. Surprisingly the scatter is smallest when one uses circular magnitudes, but the smaller elliptical magnitudes are about as good within the uncertainties.

In what follows, we adopt the magnitudes measured in circular beams.

5.2. *Velocity Widths*

Table 7 compares the Tully-Fisher scatter for ΔV measured at the 20% and 50% levels (ΔV_{20} and ΔV_{50}—Huchtmeier & Richter 1989) and the rotational velocity width (W_R) corrected for profile shape and velocity dispersion. The latter values were computed from the ΔV_{20} values in Table 1 according to the prescription of Tully & Fouqué (1985).[8] The scatter using ΔV_{20} is the smallest. Correcting the velocity widths for noncircular

[8] For the bright galaxies in our sample, the correction essentially amounts to subtracting 38 km s^{-1} from each ΔV_{20}, although the exact formula was used.

TABLE 7

LEAST-SQUARES-FIT RESULTS

Magnitude Type (1)	Velocity Width (2)	Inclination (3)	Sample (4)	Npts (5)	χ^2_{red} (6)	Δ(mag) (7)	Slope (8)	Intercept (9)	Alt. Δ(mag) (10)
Baseline:									
$H_c^{-0.5}$	ΔV_{20}	pg	$i_{pg} \geq 45°$	22	3.50	0.46	−0.105	2.547	0.37
Changing Magnitude Type:									
$H_e^{-0.5}$	ΔV_{20}	pg	$i_{pg} \geq 45°$	22	4.00	0.47	−0.100	2.548	0.40
$H_e^{0.5}$	ΔV_{20}	pg	$i_{pg} \geq 45°$	22	4.21	0.50	−0.093	2.592	0.43
H_{19}	ΔV_{20}	pg	$i_{pg} \geq 45°$	22	4.55	0.58	−0.098	2.525	0.52
Changing Velocity Width Type:									
$H_c^{-0.5}$	ΔV_{50}	pg	$i_{pg} \geq 45°$	22	5.23	0.50	−0.119	2.506	0.44
$H_c^{-0.5}$	W_R	pg	$i_{pg} \geq 45°$	22	4.59	0.49	−0.113	2.500	0.43
Changing Inclinations:									
$H_c^{-0.5}$	ΔV_{20}	IR	$i_{pg} \geq 45°$	22	3.51	0.52	−0.099	2.550	0.40
$H_e^{0.5}$	ΔV_{20}	IR	$i_{pg} \geq 45°$	22	3.92	0.52	−0.092	2.554	0.42
Changing Sample Size:									
$H_c^{-0.5}$	ΔV_{20}	pg	All	31	2.73	0.43	−0.103	2.550	0.28
$H_c^{-0.5}$	ΔV_{20}	pg	$i_{pg} \geq 60°$	14	4.73	0.47	−0.109	2.541	0.42
$H_c^{-0.5}$	ΔV_{20}	IR	All	31	3.43	0.63	−0.096	2.548	0.46
$H_c^{-0.5}$	ΔV_{20}	IR	$i_{pg} \geq 60°$	14	4.44	0.50	−0.103	2.545	0.44
Without X Cloud Galaxies:									
$H_c^{-0.5}$	ΔV_{20}	pg	All	27	2.68	0.42	−0.109	2.555	0.27
$H_c^{-0.5}$	ΔV_{20}	pg	$i_{pg} \geq 45°$	19	3.49	0.44	−0.110	2.551	0.36
Without NGC 4312 and 4419:									
$H_c^{-0.5}$	ΔV_{20}	pg	$i_{pg} \geq 45°$	20	1.86	0.30	−0.098	2.562	0.00

KEY TO COLUMNS.—(1) Type of H-magnitude (Table 3); (2) velocity widths from Table 1 (ΔV_{20} or ΔV_{50}) or corrected for noncircular motion (W_R) according to the prescription of Tully & Fouqué (1985); (3) type of inclinations (Table 4); (4) selection criterion for sample; (5) number of galaxies used; (6) reduced χ^2 of fit; (7) additional uncertainty in the H-magnitudes necessary to bring χ^2_{red} to unity if the uncertainty in the inclinations is 5°; (8) and (9) best-fit slope and intercept for $\log \Delta V = a(H - 9.0) + b$. The uncertainties in the slopes are very close to 0.013 for all fits, and the uncertainties in the intercepts are close to 0.014; (10) additional uncertainty in the H-magnitudes necessary to bring χ^2_{red} to unity if the observational uncertainty in the inclinations is 9°.

motions (W_R) does not reduce the scatter, but our sample does not include galaxies with small enough velocity widths to provide a real test of the correction. In other parts of this paper, we use ΔV_{20} unless otherwise stated.

5.3. *Inclinations*

Since galaxies at low and high inclinations should fit the same Tully-Fisher relation, we can use the degree of discrepancy to judge the inclinations derived by different methods. Figure 6 compares infrared with photographic inclinations. With photographic inclinations, there is an apparent systematic difference between galaxies with $i_{pg} > 60°$ and those of lower inclination, with 12 out of 17 of the latter galaxies lying below the best-fit line. With infrared inclinations, the systematic difference disappears, but two galaxies show large deviations. Table 7 gives a quantitative comparison, which shows that the overall scatter is nearly the same for photographic and infrared inclinations. Thus although the infrared inclinations have systematic errors for face-on galaxies, they can be used for Tully-Fisher purposes if the galaxy inclinations are known a priori to exceed 45°. If, however, infrared inclinations are to be used to *select* a high-inclination sample, the cutoff should not be less than 50°.

The Tully-Fisher relation provides an independent estimate of the inclination uncertainties. If the uncertainties are accurately estimated, the derived intrinsic scatter in the galaxy

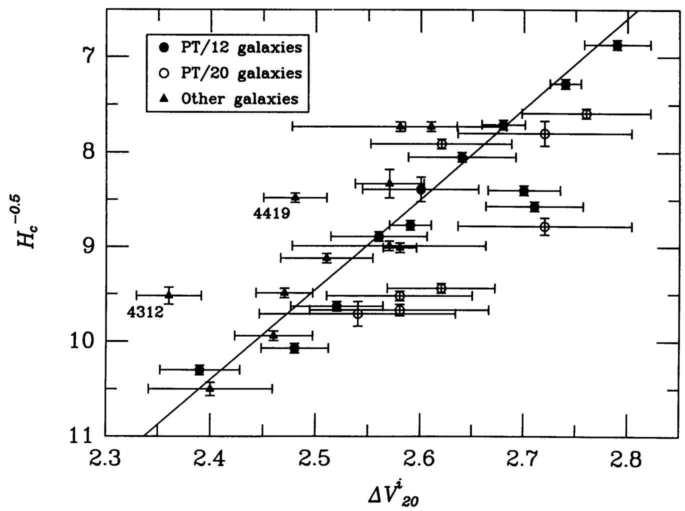

FIG. 7.—Tully-Fisher relation for galaxies in the PT sample compared to other galaxies in our sample. The infrared magnitudes in circular apertures are used together with the inclinations determined from photographic axis ratios. The 12 galaxies for which PT tabulate H-data are indicated as filled circles, the other galaxies in common with PT as open circles, and the rest of the sample of this paper as filled triangles. Vertical error bars indicate uncertainties of the observed magnitudes; horizontal error bars indicate uncertainties of the velocity widths for an assumed inclination uncertainty of 5°. The line indicates the best-fitting Tully-Fisher relation for galaxies having $i_{pg} \geq 45°$. Two of the most discrepant galaxies are labeled with their NGC numbers.

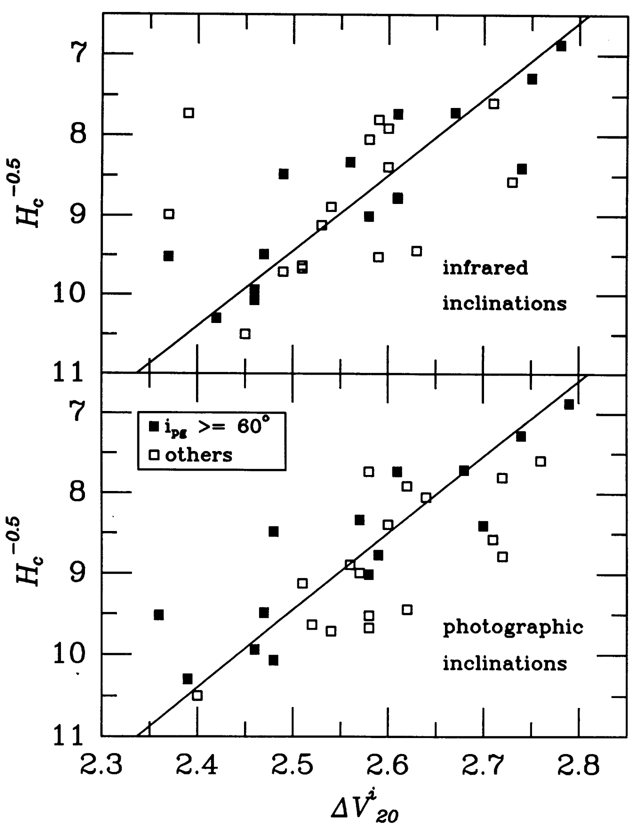

FIG. 6.—The Tully-Fisher relation for all sample galaxies. Inclinations were determined from photographic axis ratios (*upper*) and infrared axis ratios (*lower*) (Table 4). Galaxies with photographic inclinations i_{pg} larger than 60° are indicated by filled dots, others as open dots. All velocity widths are ΔV_{20} from Table 1. The line is the fit determined for galaxies with inclinations $i_{pg} \geq 45°$.

magnitudes should be the same regardless of the inclination cutoff of the sample. Table 7 shows that the derived scatter is indeed nearly constant for cutoffs of 0°, 45°, and 60°. Changing the inclination uncertainties to 9°, on the other hand, gives a progressively higher intrinsic scatter as the inclination cutoff increases (Table 7, col. [10]), a symptom of overestimated inclination uncertainties. Inclination uncertainties larger than 5° therefore seem unlikely to account for the observed scatter.

5.4. *Intrinsic Scatter*

Figure 7 shows our final Tully-Fisher diagram for the Virgo cluster. As noted in Table 7, the scatter exceeds the amount explainable solely by the known observational uncertainties. Even if the sample is restricted to $i > 60°$, where the exact value of i hardly matters, the derived dispersion *excluding* known observational uncertainties is greater than 0.4 mag. This is greater than the 0.40 mag *total* dispersion found by PT for Virgo and much greater than the intrinsic dispersion of 0.12 mag for the subsample of 20 galaxies in common (Table 6). The contrast between our H-band dispersion and that of the PT subsample implies that most of the scatter in our sample comes from the 11 galaxies not considered by PT.[9] This comparison shows that sample selection is critical to determining dispersions. The data given by PT hint at the same conclusion in that the total dispersion in the I band (with 34 galaxies observed) is 0.48 mag.

Freedman (1990) studied a sample of five galaxies having distances measured from Cepheid variables and found the scatter in the infrared Tully-Fisher relation to be 0.15 mag. If

[9] NGC 4312 and 4402 are not in the source catalog (Tully 1988b) from which the PT list was drawn. NGC 4303, 4527, 4536, 4713, and 4808 were evidently omitted because they are farther than 6° from M 87 and NGC 4394 because it has $i < 30°$. Other galaxies omitted were NGC 4298, 4302, and 4419. The only galaxies included by PT but omitted by us are galaxies with $B_T^0 > 12$ and NGC 4212.

one allows for the uncertainty in the observables, the Tully-Fisher relation appears to have no intrinsic scatter at all, in spite of the fact that the Cepheid distances themselves are uncertain by 0.1–0.3 mag! The small scatter is presumably a quirk of small number statistics, and the actual dispersion could be as large as 0.3 or even 0.5 mag (Freedman 1990). PT found a similarly small dispersion for the Ursa Major cluster. If further work confirms the small intrinsic dispersion, the scatter we measure in Virgo would have to be attributed to dispersion in the galaxy distances rather than dispersion in their intrinsic brightnesses, as suggested, for example, by Tully & Shaya (1984) and PT.

Explanations for the scatter in the galaxy H-magnitudes might include:

1. Lack of H I or sensitivity to detect the H I may make the velocity width an unreliable tracer of the galaxy mass. Haynes & Giovanelli (1986) found a population of H I–deficient spirals in the Virgo Cluster. The misleading H I spectrum in NGC 4569 (Stauffer et al. 1986) has already been mentioned, though Guhathakurta et al. (1988) found that better sensitivity almost doubled the measured velocity width for this galaxy. The latter authors also found that nearly all galaxies, in or outside the cluster, have detectable H I up to the maximum rotation velocity and fit a Tully-Fisher relation. The only gross exception in their sample is NGC 4388, which we have excluded on account of its interaction. Our sample also excludes galaxies whose H I position-velocity diagrams look disturbed or seem not to reach the full extent of the rotation curve (Table 2).

In spite of our efforts to exclude galaxies with possibly discrepant H I properties, the two most discrepant galaxies in our sample, NGC 4312 and 4419, are the two with the smallest H I fluxes. Their position-velocity diagrams (Helou et al. 1984; Hoffman et al. 1989) look regular, and the true velocity widths would have to be $\sim$80–90 km s^{-1} wider than observed to bring these galaxies into agreement. An increase this large seems unlikely, but it would be worth observing these galaxies

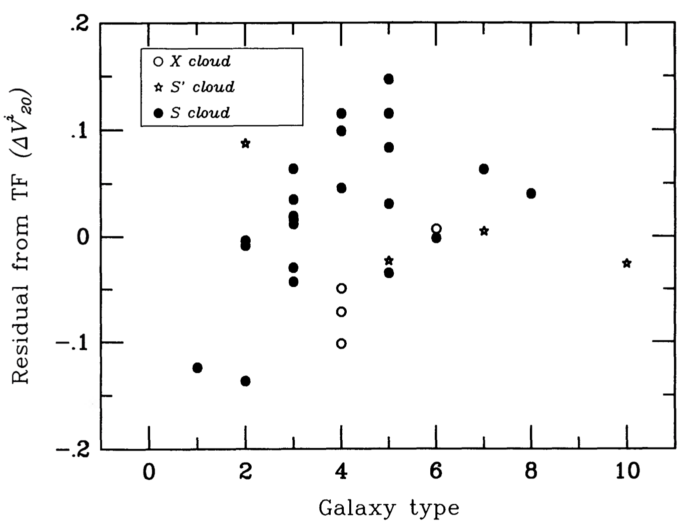

FIG. 8.—Velocity width residuals from the Tully-Fisher relation of Fig. 7 plotted against galaxy type (de Vaucouleurs & Pence 1979). Open circles denote galaxies in the X cloud (Table 1), stars denote galaxies in the S′ cloud, and filled circles denote S-cloud galaxies. A positive residual indicates that the velocity width is too large for the observed brightness or that the galaxy is too faint for its observed velocity width. The X cloud galaxies have predominately negative residuals, suggesting a smaller distance.

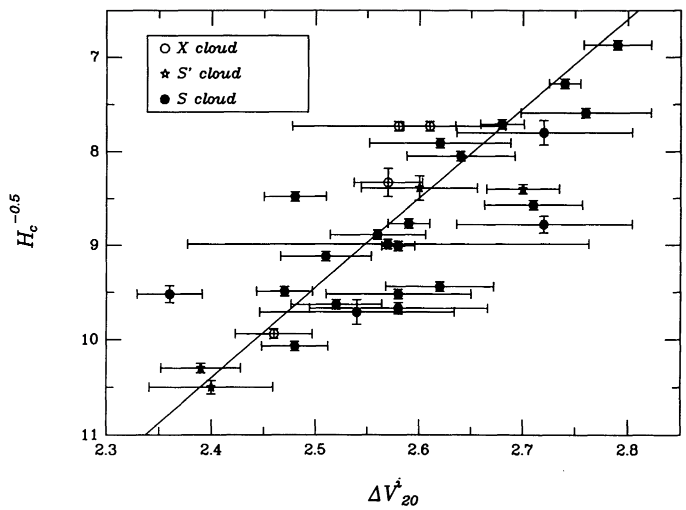

FIG. 9.—Same figure as Fig. 7 but now with the different symbols for the various clouds in the Virgo cluster. Galaxies in the X cloud are indicated as open circles, galaxies in the S′ cloud as stars, and the S-cloud galaxies as filled circles.

with better sensitivity. Even if these galaxies are omitted, the intrinsic dispersion is still 0.3 mag (Table 7).

A problem from lack of H I would probably cause a dependence of the Tully-Fisher law on galaxy type, but Figure 8 shows that there is no type dependence in the residuals, in agreement with Aaronson & Mould (1986) and PT. Bottinelli et al. (1988a) show that type effects can also result from selection bias, so there is at present no evidence that the H I width fails to trace galaxy mass.

2. Foreground or background galaxies might contaminate the sample. PT found greater dispersion in the Virgo Cluster than in the Ursa Major Cluster and attributed the excess to a population of infalling galaxies (Tully & Shaya 1984). Tonry et al. (1990) suggested that two out of 13 elliptical galaxies observed in the area of the cluster are in the foreground. Figure 9 shows the Tully-Fisher diagram with cloud assignments indicated. There is no indication in our data that the S′ or X cloud galaxies have different distances than the S cloud.

Figure 10 shows the velocity residuals as a function of radial velocity. The residuals show no velocity dependence except possibly for two galaxies near zero velocity, NGC 4312 and 4419. These two galaxies are among the three not previously assigned to the S cloud (de Vaucouleurs 1982; de Vaucouleurs & Corwin 1986), but NGC 4419 was considered a cluster member by Tully & Shaya (1984), though these authors did not mention NGC 4312. Both these galaxies have radial velocities near zero, difficult to reconcile with foreground location. As noted above, excluding them fails to eliminate most of the dispersion. Additional clusters should certainly be observed to compare their scatter with that of Virgo.

3. Is the problem one of measuring total magnitudes? All infrared studies to date only measure the light inside a diameter of $\sim 0.5D_0$, and it is possible that scatter would be reduced if total magnitudes H_T or at least magnitudes in larger beam sizes were used. BM found that the beam size can affect the scatter because galaxy surface brightness profiles differ. They also found magnitudes in beams $\approx D_0$ to be better than total magnitudes in the I band. In any case, the possibility that better magnitudes might be developed does not address the question of scatter in the magnitudes used now.

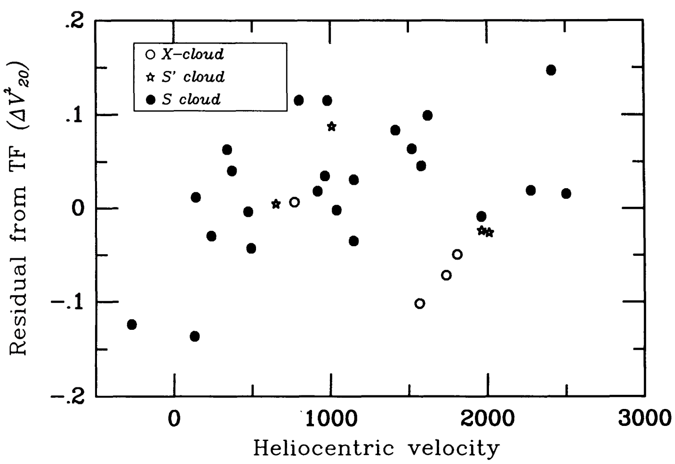

FIG. 10.—Residuals from the Tully-Fisher relation from Fig. 9 plotted against heliocentric velocity. The same symbols have been used as in Fig. 9. Velocity corrections to the center of the Local Group and for Virgo infall are essentially constant for all Virgo cluster members and need not be applied for our purposes. There is no dependence of residual on velocity except for the two low-velocity galaxies NGC 4312 and 4419, which are too bright, too nearby, or have velocity widths that are too small compared to most of the sample. The S′ and X clouds do not seem to stand out in this diagram.

4. Intrinsic M/L ratio variations are common in the optical (e.g., Kent 1986), but not much is known with regard to the infrared. Population and age differences do affect infrared colors (e.g., Aaronson, Frogel, & Persson 1978) although less than in the visible. For stellar populations of a single age and metallicity, M/L_H varies by a factor of 2 for metallicity (Z) between 0.001 and 0.04 and age between 2 and 20 Gyr (Peletier 1989). The main effect on the Tully-Fisher relation will be to change the slope because of the dependence of metallicity and mean stellar age on galaxy mass, but if these are not strict functions of mass or if galaxy ages differ, the scatter will increase too. Arguments like this show why the value of the slope cannot be derived theoretically in a simple way (e.g., Bottinelli et al. 1983). Variations of M/L as a result of irregular bursts of star formation or mergers are another way to explain the scatter, and multicolor observations could explore this question. Since M/L effects probably affect the sample selection, it would be better to select the sample on the basis of the infrared only, but not enough data are available at present.

5. Galaxies might contain considerable internal extinction even in H. Valentijn (1990), for example, claims that most spiral galaxies are optically thick in B. However, for the scatter to be caused by extinction, an average galaxy would need $A_H \approx 1$ mag, corresponding to $A_B \approx 7$ mag (Schultz & Wiemer 1975). This amount seems unlikely from, for example, gas/dust ratios. Moreover, in the present sample, the H surface brightness is highly correlated with inclination, implying that the galaxies are optically thin in H. This result will be discussed in more detail elsewhere (Peletier & Willner 1991).

6. Varying bulge-to-disk ratios at the same luminosity may cause scatter if bulges and disks contribute to the H-luminosity and the velocity widths in different proportions. Although bulge/disk ratio is a strong function of galaxy type, the residuals in the Tully-Fisher relation do not change significantly with type (Fig. 8; PT). The spread of bulge/disk ratios within each galaxy type could still give some scatter, but bulge/disk ratios seem unlikely to be the major contributor.

7. Active nuclei probably cannot contribute significant extra light and thus scatter. For all galaxies in our sample known to have active nuclei, published small-beam $H-K$ colors are consistent with those of normal galaxies (Willner et al. 1984) and not with strong Seyfert nuclei (Lawrence et al. 1985). It is therefore unlikely that active nuclei contribute significantly to the flux in the H band, especially in our large effective beam sizes.

8. The infrared Tully-Fisher law may have curvature (e.g., Aaronson et al. 1986). Our magnitude range for Virgo is too small for curvature to be significant.

6. CONCLUSIONS

An infrared study of a complete, (blue) magnitude-limited sample of galaxies in the Virgo cluster shows that:

1. Infrared images provide an excellent method of measuring galaxy magnitudes for use in Tully-Fisher studies. Magnitudes in circular beams gave slightly smaller scatter than elliptical or isophotal H_{19} magnitudes, but any of these can be used.

2. Useful inclinations can be derived from infrared axis ratios, but there are systematic errors for face-on galaxies. If infrared inclinations are to be used, samples should be restricted to galaxies known a priori to have $i > 45°$ or to galaxies having $i_H > 50°$. Aside from the systematic errors, there are residual uncertainties of about 5° from the fact that axis ratios in galaxies vary with radius. The restrictions above might be relaxed and the uncertainties decreased if infrared axis ratios could be measured at lower surface brightnesses.

3. Most of the observational uncertainty in Tully-Fisher distances originates from poorly known inclinations. We claim that existing inclinations have uncertainties as large as $\pm 5°$.

4. The Tully-Fisher law in the infrared is independent of galaxy type, at least for the most luminous galaxies, in agreement with most previous results.

5. It is very important to use a well-chosen sample when calibrating the Tully-Fisher law. Biased samples can cause the scatter to be over or underestimated.

6. Some scatter in the Tully-Fisher relation in Virgo is intrinsic. On top of the known uncertainties in the observables, the indicated magnitude dispersion in the Tully Fisher relation in the Virgo cluster is $\approx$0.4 mag or perhaps $\approx$0.3 mag if NGC 4312 and 4419 should be omitted.

Even though there is a considerable intrinsic scatter in the Tully-Fisher relation, it is tight enough to remain the best way of determining distances for large numbers of distant spirals. This study shows that one has to be extremely careful using the relation, particularly with respect to the following:

1. The inclination must be known accurately and preferably be large so that the uncertainty in sin(i) is small.

2. Samples must be chosen in an unbiased way or else the bias must somehow be corrected.

We thank M. Franx for providing the GALPHOT program and instructions on its use and R. Schild for providing the CCD image shown in Figure 5. We also thank J. Huchra, S. Kent, M. Pierce, M. Rupen, and R. B. Tully for discussions. W. Forrest, A. Fowler, and J. Pipher provided advice on the use of infrared arrays, and J. Geary, C. Hughes, and W. Wyatt constructed major parts of the SONIC. D. Mink's help with IRAF was invaluable. This research was partially supported by grants from the Scholarly Studies Fund of the Smithsonian Institution.

REFERENCES

Aaronson, M., Bothyn, G., Mould, J. R., Huchra, J., Schommer, R. A., & Cornell, M. E. 1986, ApJ, 302, 536

Aaronson, M., Frogel, J. A., & Persson, J. E. 1978, ApJ, 220, 442

Aaronson, M., et al. 1982b, ApJS, 50, 241

Aaronson, M., Huchra, J. P., & Mould, J. R. 1979, ApJ, 229, 1 (AHM)

Aaronson, M., Huchra, J., Mould, J., Schechter, P. L., & Tully, R. B. 1982a, ApJ, 258, 64

Aaronson, M., & Mould, J. 1986, ApJ, 303, 1

Aaronson, M., Mould, J., & Huchra, J. 1980, ApJ, 237, 655 (AMH)

Begeman, K. 1987, Ph.D. thesis, Univ. Gröningen

Binggeli, B., Sandage, A., & Tammann, G. A. 1985, AJ, 90, 1681

Binggeli, B., Tammann, G. A., & Sandage, A. 1987, AJ, 94, 251

Bothun, G. D., & Mould, J. R. 1987, ApJ, 313, 629 (BM)

Bothun, G. D., Mould, J., Schommer, R. A., & Aaronson, M. 1985, ApJ, 291, 586

Bottinelli, L., Fouqué, P., Gouguenheim, L., Paturel, G., & Teerikorpi, P. 1987, A&A, 181, 1

Bottinelli, L., Gouguenheim, L., Paturel, G., & de Vaucouleurs, G. 1983, A&A, 118, 4

Bottinelli, L., Gouguenheim, L., Paturel, G., & Teerikorpi, P. 1986, A&A, 156, 157

———. 1988a, ApJ, 328, 4

Bottinelli, L., Gouguenheim, L., & Teerikorpi, P. 1988b, A&A, 196, 17

Burstein, D., & Raychaudhury, S. 1989, ApJ, 343, 18

Cameron-Reed, B. 1989, Am. J. Phys., 57, 642

Danver, C.-G. 1942, Ann. Obs. Lund, No. 10

de Vaucouleurs, G. 1982, ApJ, 253, 520

de Vaucouleurs, G., & Corwin, H. G., Jr. 1986, AJ, 92, 722

de Vaucouleurs, G., & de Vaucouleurs, A. 1973, A&A, 28, 109

de Vaucouleurs, G., de Vaucouleurs, A., & Corwin, H. G., Jr. 1976, Second Reference Catalog of Bright Galaxies (Austin: Univ. Texas Press) (RC2)

de Vaucouleurs, G., & Pence, W. D. 1979, ApJS, 40, 425

Elias, J. H., Frogel, J. A., Matthews, K., & Neugebauer, G. 1982, AJ, 87, 1029

Fagerholm, E. 1906, Inaugural diss., Uppsala Univ.

Fouqué, P., Bottinelli, L., Gouguenheim, L., & Paturel, G. 1990, ApJ, 349, 1

Freedman, W. L. 1990, ApJ, 355, L35

Ftaclas, C., Fanelli, M. N., & Struble, M. F. 1984, ApJ, 282, 19

Grosbøl, P. J. 1985, A&AS, 60, 261

Groth, E. J., Juszkiewicz, R., & Ostriker, J. P. 1989, ApJ, 346, 558

Guhathakurta, P., van Gorkom, J. H., Kotanyi, C. G., & Balkowski, C. 1988, AJ, 96, 851

Haynes, M. P., & Giovanelli, R. 1986, ApJ, 306, 466

Heidmann, J., Heidmann, N., & de Vaucouleurs, G. 1971, MNRAS, 75, 85

Helou, G., Hoffman, G. L., & Salpeter, E. E. 1984, ApJS, 55, 433

Hoffman, G. L., Lewis, B. M., Helou, G., Salpeter, E. E., & Williams, H. L. 1989, ApJS, 69, 65

Hubble, E. P. 1926, ApJ, 64, 321

Huchtmeier, W. K., & Richter, O.-G. 1989, H I Observations of Galaxies (Berlin: Springer)

Kenney, J. D., & Young, J. S. 1988, ApJS, 66, 261

Kent, S. M. 1986, AJ, 91, 1301

Kraan-Korteweg, R. C., Cameron, L. M., & Tammann, G. A. 1986, in Galaxy Distances and Deviations from Universal Expansion, ed. B. F. Madore & R. B. Tully (Dordrecht: Reidel), 65

———. 1988, ApJ, 331, 620 (KCT)

Lawrence, A., Ward, M., Elvis, M., Fabbiano, G., Willner, S. P., Carleton, N., & Longmore, A. 1985, ApJ, 291, 117

Lewis, B. M. 1987, ApJS, 63, 515

Lynden-Bell, D., Faber, S. M., Burstein, D., Davies, R. L., Dressler, A., Terlevich, R. J., & Wegner, G. 1988, ApJ, 326, 19

Mould, J., Aaronson, M., & Huchra, J. 1980, ApJ, 238, 458

Ostriker, J. P., & Suto, Y. 1990, ApJ, 348, 378

Peletier, R. 1989, Ph.D. thesis, Univ. Gröningen

Peletier, R. F., & Willner, S. P. 1991, AJ, submitted

Pierce, M. J., & Tully, R. B. 1988, ApJ, 330, 579 (PT)

Richter, O.-G., & Huchtmeier, W. K. 1984, A&A, 132, 253

Richter, O.-G., Tammann, G. A., & Huchtmeier, W. K. 1987, A&A, 171, 33

Rubin, V. C., Whitmore, B. C., & Ford, W. K., Jr., 1988, ApJ, 333, 522

Sandage, A. 1988, ApJ, 331, 605

Sandage, A., & Tammann, G. A. 1981, A Revised Shapley-Ames Catalog of Bright Galaxies (Washington: Carnegie Institution)

Schechter, P. L. 1980, AJ, 85, 801

Schultz, G. V., & Wiemer, W. 1975, A&A, 43, 133

Stauffer, J. R., Kenney, J. D., & Young, J. S. 1986, AJ, 91, 1286

Teerikorpi, P. 1984, A&A, 141, 407

———. 1987, A&A, 173, 39

Tonry, J. L., Ajhar, E. A., & Luppino, G. A. 1990, AJ, 100, 1416

Tully, R. B. 1972, MNRAS, 159, 35P

———. 1988a, Nature, 334, 209

———. 1988b, Nearby Galaxies Catalog (Cambridge: Cambridge Univ. Press)

Tully, R. B., & Fisher, J. R. 1977, A&A, 54, 661

Tully, R. B., & Fouqué, P. 1985, ApJS, 58, 67

Tully, R. B., & Shaya, E. J. 1984, ApJ, 281, 31

Valentijn, E. A. 1990, Nature, 346, 153

Warmels, R. H. 1988, A&AS, 72, 19

Warner, P. J. 1973, MNRAS, 163, 163

Willner, S. P., Ward, M., Longmore, A., Lawrence, A., Fabbiano, G., & Elvis, M. 1984, PASP, 96, 143